dynamics

MDPI

Article

Numerical Analysis of the Nonlinear Dynamics of an Analog Model of a Cutting Process Involving a Shape-Memory Alloy Under Ideal and Non-Ideal Excitations

Angelo M. Tusset [1,*], Danilo Inácio [1], Jose M. Balthazar [2], Valderice H. Junkes [3] and Giane G. Lenzi [1]

[1] Department of Production Engineering, Federal University of Technology—Paraná (UTFPR), Ponta Grossa 84017-220, Brazil; daniloinacio@alunos.utfpr.edu.br (D.I.); gianeg@utfpr.edu.br (G.G.L.)
[2] Department of Mechanical Engineering, São Paulo State University (UNESP), Bauru 17033-360, Brazil; jmbaltha@gmail.com
[3] Department of Production Engineering, Paraná State University (UNESPAR), Paranagua 83203-560, Brazil; valderice.junkes@unespar.edu.br
* Correspondence: tusset@utfpr.edu.br

Abstract

This study investigates the nonlinear dynamics of a system analogous to a machining process that incorporates a shape-memory alloy (SMA) into the cutting tool structure, considering both ideal and non-ideal sources of excitation and disregarding the time-delay term related to chip thickness. Numerical simulations reveal chaotic behavior for specific parameter combinations, as evidenced by time series, phase portraits, Poincaré maps, bifurcation diagrams, Lyapunov exponents, and the 0–1 test for chaos. A systematic comparison of ideal and non-ideal excitation is conducted to assess their respective effects on the system's dynamic response and chaotic behavior. Furthermore, the results demonstrate that variations in the SMA temperature significantly affect the tool's vibrational response and can alter the system's dynamic regime. To reduce vibration amplitudes and mitigate the impact of temperature fluctuations, a time-delayed control (TDC) strategy is proposed. The robustness of the controller is evaluated under various SMA temperature conditions, examining its ability to suppress chaotic oscillations and maintain periodic system behavior. Numerical results show that the proposed TDC strategy effectively reduces vibration amplitudes and suppresses chaotic dynamics, while maintaining periodic or quasi-periodic responses across the investigated temperature variations. These findings underscore the importance of accounting for the characteristics of the excitation source and the SMA's thermal conditions when designing vibration control strategies for machining systems.

Keywords: nonlinear dynamics; non-ideal excitation; chaotic behavior; time-delayed control

Check for updates

Academic Editor: Christos Volos

Received: 18 October 2026
Revised: 19 November 2026
Accepted: 22 November 2026
Published: 25 November 2026

Copyright: © 2026 by the authors. Licensee MDPI, Basel, Switzerland. This article is an open access article distributed under the terms and conditions of the Creative Commons Attribution (CC BY) license.

1. Introduction

The occurrence of vibrations during machining operations is a major factor limiting the performance of manufacturing processes. These vibrations can compromise the surface quality of parts, reduce dimensional accuracy, accelerate cutting tool wear, and consequently lower process productivity. In more critical situations, dynamic instability can significantly restrict permissible cutting conditions, thereby limiting operational efficiency. Given these impacts, the development of strategies to mitigate vibrations and enhance the stability of machining processes has attracted growing interest from both the scientific community and the industrial sector [1].

The primary sources of vibrations in cutting operations include frictional interactions at the tool–workpiece interface and regenerative effects arising from process dynamics. Friction-induced vibrations arise from mechanical interactions within the contact zone. In contrast, regenerative vibrations arise from the dependence of the cutting force on the instantaneous chip thickness, which is determined by the difference between the current and previous positions of the tool and the machined surface. This dependency introduces a memory effect into the system's dynamics, which can trigger self-excited instabilities known as regenerative chatter [2–4].

Mathematically representing these phenomena often requires nonlinear models that can capture the dynamic characteristics observed during the cutting process. In this context, models based on the Duffing oscillator have been employed to investigate nonlinear vibration responses, bifurcations, and transitions to chaotic behavior in machining systems, particularly when the structural dynamics exhibit nonlinear stiffness [5]. Furthermore, excitation sources arising from geometric imperfections, residual eccentricities, and interactions between the structure and the drive system can significantly alter the dynamic response and stability of the process [6]. Structural parameters, such as stiffness and damping, also directly influence vibration characteristics and operational stability limits [7].

The significance of structural nonlinearities is particularly evident in robotic machining, where joint flexibility and dynamic characteristics can affect process stability. Reference [8] presents an investigation into chatter during milling operations performed by industrial robots, explicitly accounting for stiffness and damping nonlinearities in the robot joints. The results demonstrate that these effects can play a crucial role in predicting dynamic behavior and determining stable cutting conditions.

Given the technical and economic impacts of vibrations, various control strategies have been developed to extend the stable operating range and enhance the performance of machining processes. These strategies can be broadly classified as passive, active, or semi-active. Passive systems utilize mechanical elements that absorb or dissipate vibrational energy, such as dynamic absorbers, friction dampers, and tuned mass dampers [9,10]. Although they offer advantages regarding design simplicity and implementation costs, their performance may be limited when faced with variations in operating conditions and system dynamic parameters [11].

Active control systems, in turn, utilize sensors, actuators, and control algorithms to modify the system's dynamic response by applying control forces. The efficiency of these strategies depends on actuator capabilities, the availability of information regarding the system state, and the controller's robustness against disturbances, parametric uncertainties, and physical limitations. Semi-active systems, meanwhile, modify mechanical properties, such as stiffness or damping, via adjustable mechanisms, without necessarily applying direct mechanical control forces. In this context, smart materials and adaptive damping devices represent promising alternatives for vibration control in machining processes [9,10].

Among the proposed active strategies, Ref. [12] investigated a damping system based on magnetorheological (MR) fluid, integrated into a boring bar and controlled by a Variable Gain Super-Twisting Sliding Mode strategy. The controller was used to regulate the damping force and attenuate regenerative vibrations. Numerical and experimental results indicated improved process stability across various machining conditions, highlighting the potential of nonlinear control techniques to handle disturbances and parametric uncertainties.

In [13], an active feedback strategy for suppressing chatter-type vibrations during milling operations is presented. The methodology employs a response matrix to represent process dynamics and accounts for parameters such as feed rate, tooth-passing frequency, and time-varying dynamic cutting-force coefficients. The results demonstrate

the potential of active control to reduce vibrations and improve the dynamic behavior of the milling process.

Other approaches seek to directly modify the dynamic properties of the workpiece or the machining assembly. In [14], a mobile support technology, termed "follow-up support," is proposed to reduce vibrations during the milling of thin-walled components. The device provides stiffness and damping near the cutting zone, altering the workpiece dynamics during the operation. A combination of regenerative instability modeling, stability diagram analysis, and experimental testing demonstrated the approach's potential to expand the stable operating range and improve surface quality.

Regarding instability identification, Ref. [15] investigated chatter detection techniques in milling, including signal processing, time-frequency analysis, feature extraction, and the classification of machining conditions. Instability detection is a crucial step for control architectures that integrate process monitoring with the activation of mitigation devices, such as piezoelectric actuators and smart damping systems. However, chatter identification and effective chatter suppression are distinct challenges that require complementary monitoring and control strategies.

More recently, Ref. [16] proposed a semi-active vibration-attenuation device combined with mobile support technology for milling thin-walled components. The approach combines localized stiffness enhancement with targeted vibration reduction, aiming to control workpiece deformation and regenerative instability simultaneously. In [17], a smart clamping and damping device for the robotic machining of thin-walled components was investigated, integrating a flexible structure with a magnetorheological damping module. In this system, the clamping position and tangential stiffness are adjusted to modify the dynamics of the tool–workpiece–fixture assembly. In [18], an analysis of a vibration absorber based on a Spiral Acoustic Black Hole (ABH) is presented, exploring its absorption mechanism and its effects on vibration and dynamic stability during the milling of thin-walled components.

Despite the advances achieved, the practical implementation of active control systems also presents limitations. In [19], the effects of actuator saturation on active vibration control during milling are studied, combining analytical modeling, frequency analysis, and machining experiments. This aspect is significant because actuator physical characteristics limit the available control force; consequently, controller performance may be compromised when the compensation demand exceeds the device's operational limits.

Among the smart materials used for vibration control, shape memory alloys (SMAs) are of particular interest due to their ability to change their mechanical properties in response to temperature changes and phase transformations. This characteristic enables the development of adaptive structures whose stiffness and dynamic response can be adjusted according to operating conditions. When temperature is used solely as an analysis parameter, the influence of the SMA can be investigated as a thermomechanical adaptation mechanism of the structure. On the other hand, when a controlled heating system deliberately modifies temperature, its regulation becomes an additional actuation strategy that must account for the thermal dynamics and energy requirements involved. In [11], the use of these alloys in cutting tools is discussed, highlighting their potential to reduce vibration, improve surface quality, and enhance process stability.

In this context, Ref. [20] investigated a friction damper made of copper-based shape memory alloys, applied to a boring bar. The study considered various alloys, including naval brass, Muntz metal, and leaded brass, aiming to reduce chatter associated with the low stiffness of slender tools. The results highlight the potential of friction damping based on shape memory alloys as an alternative for modifying the dynamic response of machining tools. However, leveraging the temperature dependence of SMA mechanical properties,

combined with an active control strategy, offers an additional avenue for enhancing vibration mitigation capabilities.

Another relevant aspect in analyzing machining tool dynamics is the nature of the excitation source. In systems with ideal excitation, the motion or excitation frequency is prescribed and remains unaffected by the structure's vibrational response. In contrast, in systems with non-ideal excitation, the driving source possesses its own dynamics and can interact with the excited structure, meaning tool vibrations affect the power source's operation. This interaction can alter response frequency and amplitude, introduce additional energy transfer mechanisms, and modify stability conditions. Therefore, considering non-ideal excitation sources enables representation of operating conditions in which the coupling between the drive mechanism and the structure plays a significant role in the system's dynamic behavior. Comparing ideal and non-ideal excitations thus enables investigation of whether a control strategy's effectiveness remains consistent when the power source dynamics are incorporated into the model.

Beyond reducing vibration amplitudes, analyzing nonlinear machining systems may require investigating periodic, quasi-periodic, and chaotic regimes. Although a reduction in vibration amplitude indicates improved dynamic performance, it does not necessarily imply the elimination of chaotic behavior. Therefore, evaluating the effectiveness of control strategies requires considering both the evolution of amplitude and dynamic indicators to identify motion regimes. Tools that can be employed for this purpose include bifurcation diagrams, Poincaré sections, Lyapunov exponents, and the 0–1 test; their use should be determined based on the mathematical formulation and available results.

Against this backdrop, this study investigates vibration control and the suppression of chaotic behavior in machining tools incorporating shape memory alloys (SMAs) into their structures. The investigation considers the influence of alloy temperature on mechanical properties and the system's dynamic response, as well as the application of an active control strategy based on the Time Delay Control (TDC) technique. The study's main contribution lies in the systematic comparison of the dynamic behavior of systems subjected to ideal versus non-ideal excitation sources; this allows for an assessment of how the interaction between the driving source and the vibrating structure influences the system response, the occurrence of chaos, and the effectiveness of control strategies.

Furthermore, the study examines the TDC controller's ability to reduce vibration amplitudes and suppress chaotic behavior, driving the system into a periodic motion regime. The analysis covers various operating conditions and accounts for changes in SMA mechanical properties resulting from temperature variations. In this context, controller robustness is evaluated by its ability to maintain the system in a periodic regime despite fluctuations in alloy temperature, considering both ideal and non-ideal excitation scenarios. This approach enables investigation of the extent to which changes in the structure's thermomechanical properties and the coupling between the driving source and the vibrating system affect the stabilization capability provided by TDC control.

The scientific contribution of this work, therefore, lies in an integrated assessment of how the nature of the excitation source, SMA temperature variations, and the application of TDC (time-delay control) influence the nonlinear dynamics of machining tools. A systematic comparison between systems with ideal and non-ideal excitation allows identification of differences in vibrational response and process dynamics. At the same time, a robustness analysis evaluates whether the controller can maintain a periodic regime when the alloy's mechanical properties are temperature-dependent. In this way, the study contributes to understanding the possibilities and limitations of TDC in suppressing chaotic behavior and maintaining the dynamic stability of mechanical systems characterized by

variable thermomechanical properties and by coupling between the excitation source and the structure.

The organization of this paper is as follows. Section 2 presents the mathematical models of the system, the methodology for developing the controller using the Time Delay Control (TDC) technique, and the procedure for applying the Lyapunov exponent, and the 0–1 test to identify chaotic behavior. Section 3 presents the numerical simulation results, including an analysis of how temperature variations in the shape memory alloy influence system dynamics. Furthermore, the proposed control strategy is evaluated by investigating its effectiveness in reducing cutting tool vibration amplitudes and suppressing chaotic behavior. Finally, the work's conclusions and main contributions are presented in Section 4.

2. Materials and Methods

2.1. Mathematical Model

Figure 1 illustrates a simplified physical model of the orthogonal machining process that accounts for the cutting tool's vibratory dynamics and the system's rotational motion. The model is a system representing the cutting tool that is subject to the angular motion of the induction motor shaft, thereby forming an ideal and a non-ideal vibration system. This configuration allows investigation of the interaction among structural vibrations, cutting forces, and energy limitations imposed by the excitation source, characteristics frequently associated with nonlinear phenomena observed in machining processes.

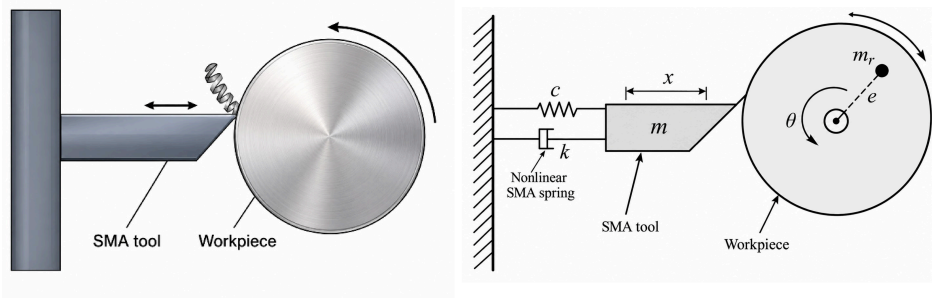

Figure 1. Physical model of the turning process. (**a**) Orthogonal turning. (**b**) Schematic diagram.

As shown in Figure 1, in this work, the cutting tool is considered to be composed of a shape memory alloy, whose stiffness can be modified by varying the temperature, allowing its use as a semi-active control. In this work, we employ the polynomial constitutive model proposed in [21] to describe the nonlinear mechanical behavior of the shape memory alloy (SMA). The selection of this formulation is primarily motivated by its ability to represent the martensitic phase transition using a temperature-dependent free-energy potential, which enables the identification of various equilibrium configurations and the investigation of the material's nonlinear mechanical response.

The parameters of the shape-memory-alloy (SMA) spring are given in Equation (1). Equation (1) represents the mathematical model of the shape memory alloy (SMA) spring force [22]:

$$k(x, T) = a\Delta T x + bx^3 + cx^5 \quad (1)$$

where $\Delta T = (T - T_M)$ is the temperature variation in the alloy, T_M is the temperature in martensitic phases, x is the compression/extension of the spring, and a, b and c are constant values. The values of the parameters a, b, and c can be estimated through experimental tests. In this work, the parameters were adjusted to approximate the behavior of an alloy composed of nickel and titanium (NiTi), for which data were obtained from [23]. Considering only the variation of ΔT variations above 77 (Kelvin), and thus limiting for

ΔT ($\Delta T_{\min} = 77$, $\Delta T_{\max} = 250$). In this work, we numerically investigate the range 77–250 K, enabling analysis of how temperature influences tool dynamics over a broader span and identifying regions of sensitivity and potential qualitative shifts in motion regimes. Considering temperatures up to 150 K enables the investigation of previously identified sensitivity regions [24]. However, limiting the analysis to this value precludes a full assessment of how the dynamic behavior evolves beyond these regions. It should be noted that the parametric analysis of temperature in this context does not necessarily reflect the thermal evolution of the tool during machining; rather, in the adopted model, it is treated as a parameter in the free-energy expression, and its variation corresponds to different constitutive conditions.

Where x is the tool chatter amplitude, m is the cutting tool mass, c is damping, k and k_{nl} are the linear and non-linear stiffness, m_0 is the unbalanced mass of the motor, and r is the eccentricity of the unbalanced mass.

In this paper, the Lagrangian equation (Equation (2)) is considered to obtain the mathematical model of Figure 1:

$$L = T - V \tag{2}$$

where T is the kinetic energy, and V is the potential energy.

The mathematical model is obtained from:

$$\frac{d}{dt}\left(\frac{\partial L}{\partial \dot{Q}_i}\right) - \frac{\partial L}{\partial Q_i} = \Im_i \tag{3}$$

where i = 1, 2, …, N. N is the degree of freedom system, $\Im_i$ are non-conservative forces, Q_i are generalized coordinates.

2.1.1. Mathematical Model for the Case of the Ideal Excitation Source

Considering that a sinusoidal excitation of the form can approximate the vibration generated by the movement of the motors:

$$F_{exc} = A_{exc} \sin(\Omega t) \tag{4}$$

where A_{exc} represents the excitation amplitude, and Ω represents the excitation frequency in radians.

Disregarding the gravitational force, the ideal system considered in Figure 1 presents the following potential energy:

$$V = \frac{a\Delta T x^2}{2} + \frac{bx^4}{4} + \frac{ex^6}{6} \tag{5}$$

Kinetic energy is obtained from:

$$T = \frac{1}{2} m \dot{x}^2 \tag{6}$$

Non-conservative energies are obtained from:

$$\Im = -c\dot{x} + A_{exc} \sin(\Omega t) \tag{7}$$

Considering the substitution of (5) and (6) in (2), and the substitution of (2) and (7) in (3), the following mathematical model is obtained:

$$m\ddot{x} + c\dot{x} + a\Delta T x + bx^3 + ex^5 = A_{exc} \sin(\Omega t), \tag{8}$$

Considering the following substitutions: $\tau = \omega t$, $\omega = \sqrt{\frac{a\Delta T}{m}}$, $x_1 = \frac{x}{x^*}$, $x_2 = \dot{x}$, $\alpha_1 = \frac{c}{\omega m}$, $\alpha_2 = \frac{a\Delta T}{\omega^2 m}$, $\alpha_3 = \frac{b}{\omega^2 m}$, $\alpha_4 = \frac{e}{\omega^2 m}$ and $\alpha_5 = \frac{A_{exc}}{\omega^2 m}$. The parameter x^* represents the characteristic displacement scale adopted in the nondimensionalization procedure.

The system (7) is obtained in dimensionless form:

$$\ddot{x}_1 = -\alpha_1\dot{x}_1 - \alpha_2 x_1 - \alpha_3 x_1^3 - \alpha_4 x_1^5 + \alpha_5 \sin(\Omega t), \tag{9}$$

The following system can represent the system (8):

$$\begin{aligned} \dot{x}_1 &= x_2 \\ \dot{x}_2 &= -\alpha_1 x_2 - \alpha_2 x_1 - \alpha_3 x_1^3 - \alpha_4 x_1^5 + \alpha_5 \sin(\Omega t), \end{aligned} \tag{10}$$

2.1.2. Mathematical Model for the Case of the Non-Ideal Excitation Source

Disregarding the gravitational force, the non-ideal system considered in Figure 1 presents the following potential energy:

$$V = \frac{a\Delta T x^2}{2} + \frac{bx^4}{4} + \frac{ex^6}{6} \tag{11}$$

Kinetic energy is obtained from [25]:

$$T = \frac{1}{2}m\dot{x}^2 + \frac{1}{2}J\dot{\theta}^2 + \frac{1}{2}m_0\left(\dot{x}^2 + r^2\dot{\theta}^2 - 2r\dot{x}\dot{\theta}\sin(\theta)\right) \tag{12}$$

where the trigonometric term represents the kinematic coupling between the translation of the support and the rotation of a motor mass [25].

Non-conservative energies are obtained from:

$$\begin{aligned} \Im_1 &= -c\dot{x} \\ \Im_2 &= V_1 - V_2\dot{\varphi} \end{aligned} \tag{13}$$

Considering the substitution of (12) and (13) in (2), and the substitution of (2) and (13) in (3), the following mathematical model is obtained:

$$\begin{aligned} &m\ddot{x} + c\dot{x} + a\Delta T x + bx^3 + ex^5 = m_0 r\ddot{\theta}\sin(\theta) + m_0 r\dot{\theta}^2\cos(\theta) \\ &\left(J + r^2 m_0\right)\ddot{\theta} - m_0 r\ddot{x}\sin(\theta) = V_1 - V_2\dot{\theta} \end{aligned} \tag{14}$$

where J is the moment of inertia for the motor, θ is angular displacement, and $V_1 - V_2\dot{\theta}$ represents the electromagnetic torque generated by the electric motor, which acts as the excitation source of the non-ideal mechanical system. In this expression, V_1 denotes the constant component associated with the voltage applied to the motor armature, whereas V_2 is the motor torque coefficient associated with the angular velocity, accounting for the variation in the electromagnetic torque as the motor speed changes [25].

Considering the following substitutions: $\tau = \omega t$, $\omega = \sqrt{\frac{a\Delta T}{m}}$, $x_1 = \frac{x}{x^*}$, $x_2 = \dot{x}$, $x_3 = \frac{\theta}{\theta^*}$, $x_4 = \dot{x}_3$, $I = J + r^2 m_0$, $\alpha_1 = \frac{c}{\omega m}$, $\alpha_2 = \frac{a\Delta T}{\omega^2 m}$, $\alpha_3 = \frac{b}{\omega^2 m}$, $\alpha_4 = \frac{e}{\omega^2 m}$, $\delta_1 = \frac{m_0 r}{m}$, $\delta_2 = \frac{m_0 r}{\omega m}$, $\beta_1 = \frac{m_0 r}{I}$, $\beta_2 = \frac{V_1}{\omega^2 I}$ and $\beta_3 = \frac{V_2}{\omega I}$. The parameter θ^* represents the characteristic angular displacement scale adopted in the nondimensionalization procedure.

The system (14) is obtained in dimensionless form:

$$\begin{aligned} \ddot{x} &= -\alpha_1\dot{x} - \alpha_2 x - \alpha_3 x^3 - \alpha_4 x^5 + \delta_1\ddot{\theta}\sin(\theta) + \delta_2\dot{\theta}^2\cos(\theta) \\ \ddot{\theta} &= \beta_1\ddot{x}\sin(\theta) + \beta_2 - \beta_3\dot{\theta} \end{aligned} \tag{15}$$

The following system can represent the system (15):

$$\begin{aligned} \dot{x}_1 &= x_2 \\ \dot{x}_2 &= \frac{1}{1+\beta_1\delta_1\sin(x_3)^2}\begin{pmatrix} -\alpha_1 x_2 - \alpha_2 x_1 - \alpha_3 {x_1}^3 - \alpha_4 {x_1}^5 \\ +\beta_2\delta_1\sin(x_3) - \beta_3 x_4\delta_1\sin(x_3) + \delta_2 {x_4}^2\cos(x_3) \end{pmatrix} \\ \dot{x}_3 &= x_4 \\ \dot{x}_4 &= \frac{1}{1+\beta_1\delta_1\sin(x_3)^2}\begin{pmatrix} -\alpha_1 x_2\beta_1\sin(x_3) - \alpha_2 x_1\beta_1\sin(x_3) \\ -\alpha_3 {x_1}^3\beta_1\sin(x_3) - \alpha_4 {x_1}^5\beta_1\sin(x_3) + \\ \delta_2 {x_4}^2\cos(x_3)\beta_1\sin(x_3) + \beta_2 - \beta_3 x_4 \end{pmatrix} \end{aligned} \tag{16}$$

2.2. Time-Delayed Feedback Control

As originally suggested by the author of [26], continuous control input stabilizing a chaotic oscillation is given by the difference between the current output and the past one as follows [27]:

$$U = K\{g[x(\tau - T), \dot{x}(\tau - T)] - g[x(\tau), \dot{x}(\tau)]\} \tag{17}$$

where T is the time delay, and K is the feedback gain.

The $g[x(\tau), \dot{x}(\tau)]$ and imply a scalar output signal measured at the current time τ, and the past time $(\tau - T)$, respectively.

Since the control input (17) only depends on the output signal, the time delay T is adjusted to the period of a target unstable periodic orbit that is intended to be stabilized in a chaotic attractor, and the control input therefore converges to null after the controlled system is stabilized to the target orbit.

Assuming that the velocity of oscillation is measured as an output of the nonlinear system (10) and (16), the control signal U is given as follows:

$$U = K[x_2(\tau - T) - x_2(\tau)] \tag{18}$$

The time delay T is adjusted to $T = \frac{2\pi}{\Omega}$, where Ω represents one of the predominant excitation frequencies.

2.3. The 0–1 Test

The 0–1 test, proposed by [28], is directly applied to the time series data, based on the statistical properties of a single coordinate (here in the variable x_1) (see Equations (10) and (16)). Basically, the 0–1 test consists of estimating a single parameter K. The test considers a system variable x_j, where two new coordinates (p,q) are defined as follows:

$$p(n, \bar{c}) = \sum_{j=0}^{n} x(j) \cos(j\bar{c}) \tag{19}$$

$$q(n, \bar{c}) = \sum_{j=0}^{n} x(j) \sin(j\bar{c}) \tag{20}$$

where $\bar{c} \in (0, \pi)$ is a constant. The mean square displacement of the new variables $p(n, \bar{c})$ and $q(n, \bar{c})$ is given by:

$$M(n, c) = \lim_{n \to \infty} \frac{1}{N} \sum_{j=1}^{N} \Big[(p(j+n, \bar{c}) - p(j, \bar{c}))^2 + (q(j+n, \bar{c}) - q(j, \bar{c}))^2 \Big] \tag{21}$$

where $n = 1, 2, \ldots, N$; therefore, we obtain the parameter K in the limit of a very long time:

$$K = \frac{\mathrm{cov}(Y, M(\bar{c}))}{\sqrt{\mathrm{var}(Y)\mathrm{var}(M(\bar{c}))}} \tag{22}$$

where vectors $M(\bar{c}) = [M(1, \bar{c}), M(2, \bar{c}), \ldots, M(n_{\max}, \bar{c})]$ and $Y = [1, 2, \ldots, n_{\max}]$.

Given any two vectors x and y, the covariance $\mathrm{cov}(x, y)$ and variance $\mathrm{var}(x)$, of $n_{\max}$ elements are usually defined as [27]:

$$\mathrm{cov}(x, y) = \frac{1}{n_{\max}} \sum_{n=1}^{n_{\max}} (x(n) - \bar{x})(y(n) - \bar{y}) \tag{23}$$

$$\mathrm{var}(x) = \mathrm{cov}(x, x) \tag{24}$$

where $\bar{x}$ and $\bar{y}$ are the average of $x(n)$ and $y(n)$, respectively. As a final result, the value of the searched parameter K is obtained by taking the median of 100 different values of the parameter $\bar{c} \in (0, \pi)$ in Equation (21). If the K value is close to 0 the system is periodic; on the other hand, if the K value is close to 1 the system is chaotic. In all simulations, it is necessary to choose $n = 10000$ and $j = \frac{n}{100}, \ldots, \frac{n}{10}$ [29].

3. Results

Numerical simulations of the system were performed using MATLAB R2025b, the ODE45 solver, based on the explicit fourth- and fifth-order Dormand–Prince Runge–Kutta method with adaptive integration step control, and RK4, with h = 0.01, implemented on an Intel i7 (3.20 GHz, six-core) with 32 GB RAM, with the following parameters: $\alpha_1 = 0.25$, $\alpha_2 = -0.012987\Delta T$, $\alpha_3 = 0.5$, $\alpha_4 = -0.006$, $\alpha_5 = 2$, $\beta_1 = 0.05$, $\beta_2 = 100$; $\beta_3 = 200$, $\delta_1 = 8.373$, $\delta_2 = 8.373$, $\Omega = 0.5$, and initial conditions $x_1 = x_2 = x_3 = x_4 = 0$.

3.1. Numerical Simulations for the Case of the Ideal Excitation Source

Figure 2 shows the variation in tool-tip displacement relative to the temperature variation in the SMA material, presenting the bifurcation diagram and the 0–1 test value.

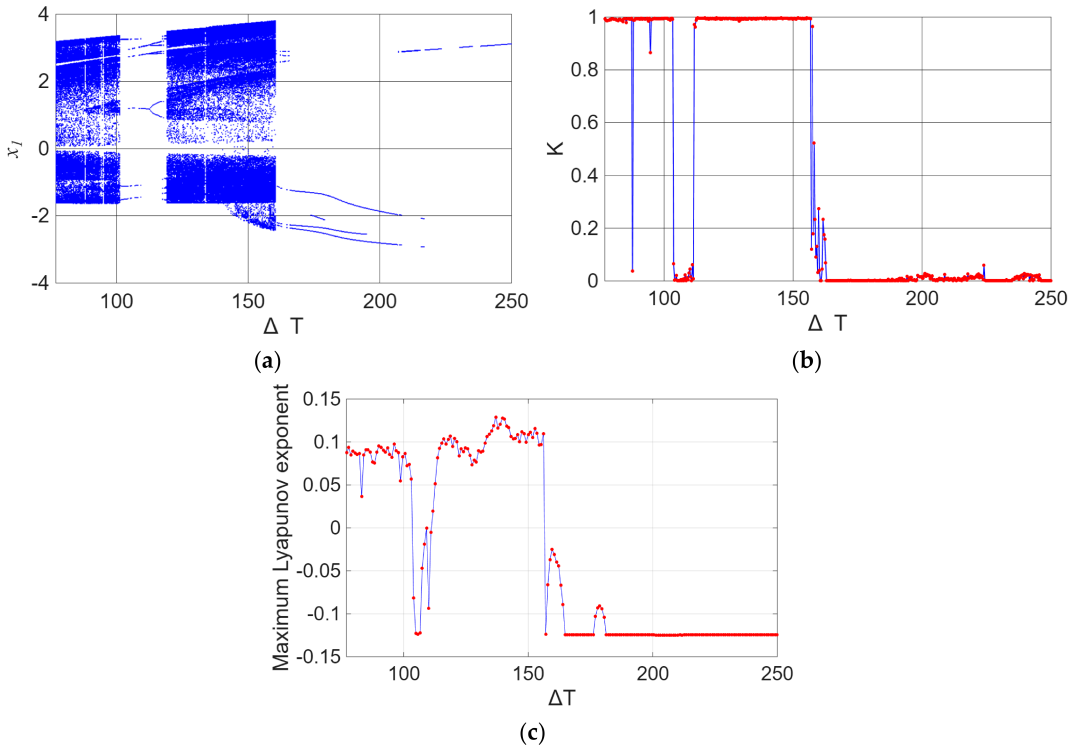

Figure 2. (**a**) Bifurcation Diagram for $\Delta T = [77 : 250]$. (**b**) 0–1 test for $\Delta T = [77 : 250]$. (**c**) Maximum Lyapunov exponent for $\Delta T = [77 : 250]$.

As shown in Figure 2, the tool temperature causes the behavior to alternate between chaotic (K close to 1, Figure 2a) and periodic (K close to 0, Figure 2a).

Figure 3 shows the time history, phase diagram, and Poincaré map for $\Delta T = 77$.

As shown in Figure 3, at ambient temperature, the tool exhibits chaotic behavior during machining; however, as shown in Figure 2, the tool's behavior can shift between periodic and chaotic states with temperature variations, provided the tool is made of SMA. If maintaining the temperature at a specific value is not feasible, the system can be controlled through active or semi-active control.

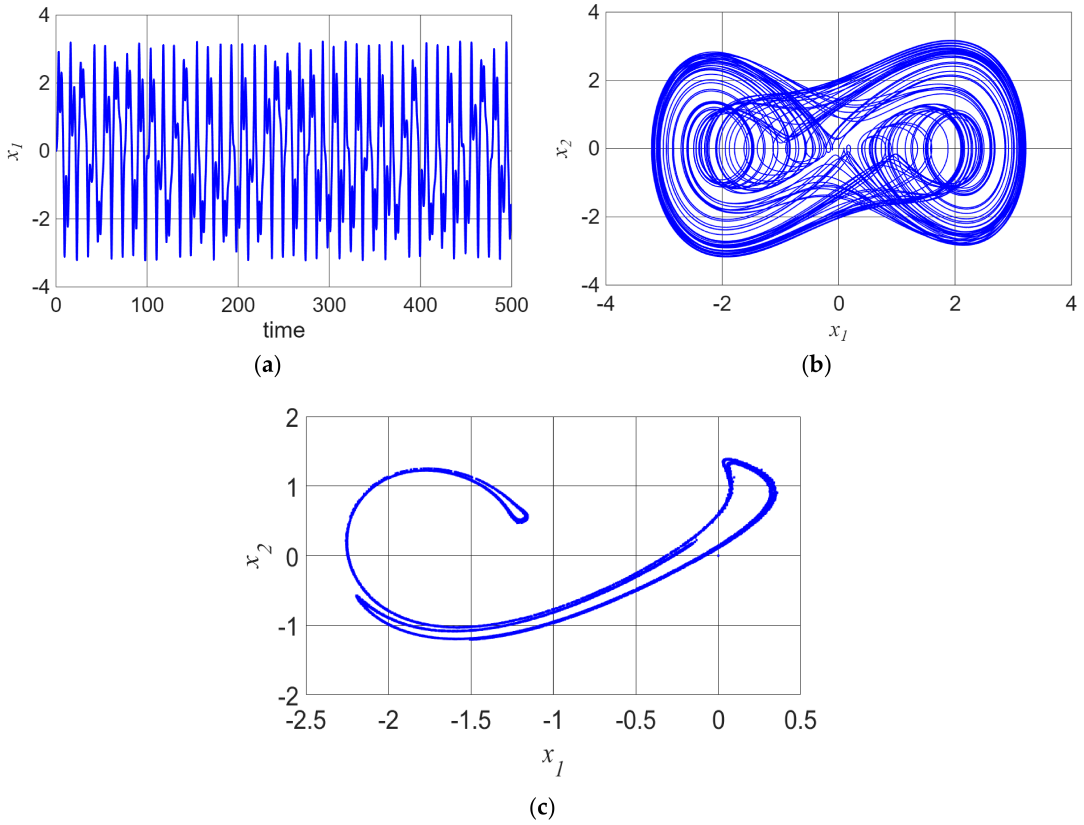

Figure 3. (**a**) Tool tip displacement (x_1) to $\Delta T = 77$. (**b**) Phase Diagram x_1 versus x_2 to $\Delta T = 77$. (**c**) Poincaré map for $\Delta T = 77$.

Application of Time-Delayed Feedback Control

Considering the inclusion of a control signal U in the system (10), in the following form:

$$\begin{aligned} \dot{x}_1 &= x_2 \\ \dot{x}_2 &= -\alpha_1 x_2 - \alpha_2 x_1 - \alpha_3 x_1^3 - \alpha_4 x_1^5 + \alpha_5 \sin(\Omega t) + U \end{aligned} \tag{25}$$

Considering the angular frequency $\Omega = 0.5$, we obtain the time delay $T = \frac{2\pi}{0.5} \approx 12.5664$.

In Figure 4, we can observe the bifurcation diagram for system (5) with control U, considering $T \approx 12.5664$ and variations in the control gain κ.

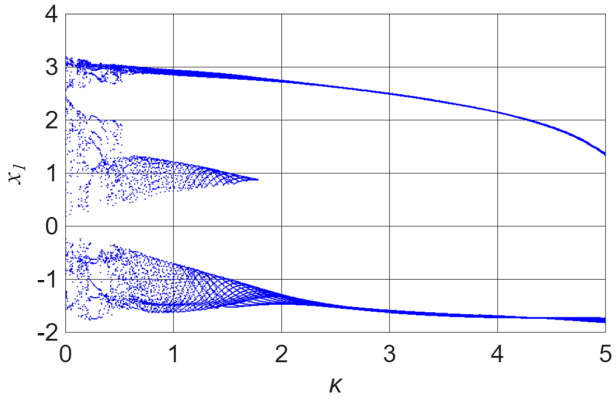

Figure 4. Bifurcation Diagram for $\kappa = [0 : 5]$.

We can observe in Figure 4 that the system with time-delay control for $T \approx 12.5664$ and $\kappa = 4.4$ shifts the system from chaotic behavior to periodic behavior. Substituting $T \approx 12.5664$ and $\kappa = 4.4$ into the system (18), we obtain the control:

$$U = 4.4[x_2(\tau - 12.5664) - x_2(\tau)] \tag{26}$$

The time delay T is adjusted to $T = \frac{2\pi}{\Omega}$, where Ω represents one of the predominant excitation frequencies.

Figure 5 presents the time history and the control signal employed for the system (25), with control (26).

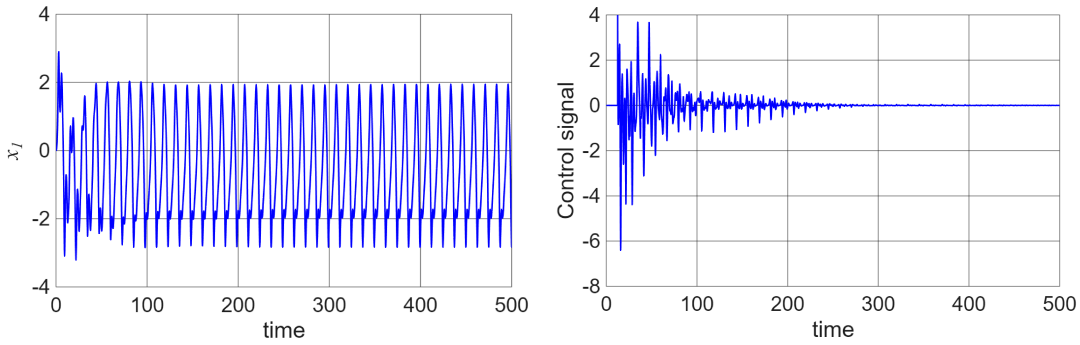

(**a**) (**b**)

Figure 5. (**a**) Time history for ideal systems with control. (**b**) The control signal is applied in the control.

Figure 6 presents the time history and phase diagram for the system, both without and with control.

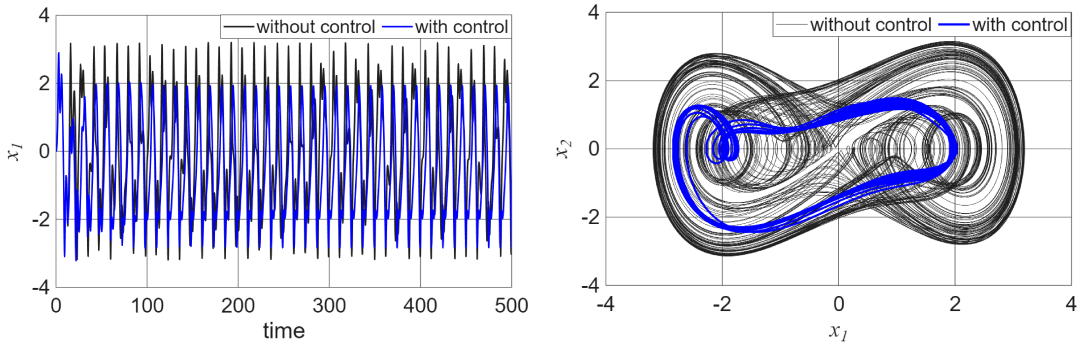

(**a**) (**b**)

Figure 6. (**a**) Time history for ideal systems without and with control. (**b**) Phase Diagram of x_1 versus x_2 for ideal systems, with and without control.

As can be observed in Figures 5 and 6, the proposed control steered the system from chaotic behavior to periodic behavior, applying only the control force necessary to stabilize the system's dynamics onto the desired periodic orbit. After approximately 250 time units, the control force tends toward zero, indicating that the periodic orbit is maintained without significant continuous intervention. Furthermore, as shown in Figure 6a, the control resulted in a 41.32% reduction in the system's displacement amplitude.

3.2. Numerical Simulations for the Case of the Non-Ideal Excitation Source

Figure 7 shows the variation in tool-tip displacement relative to the temperature variation in the SMA material, presenting the bifurcation diagram and the 0–1 test value.

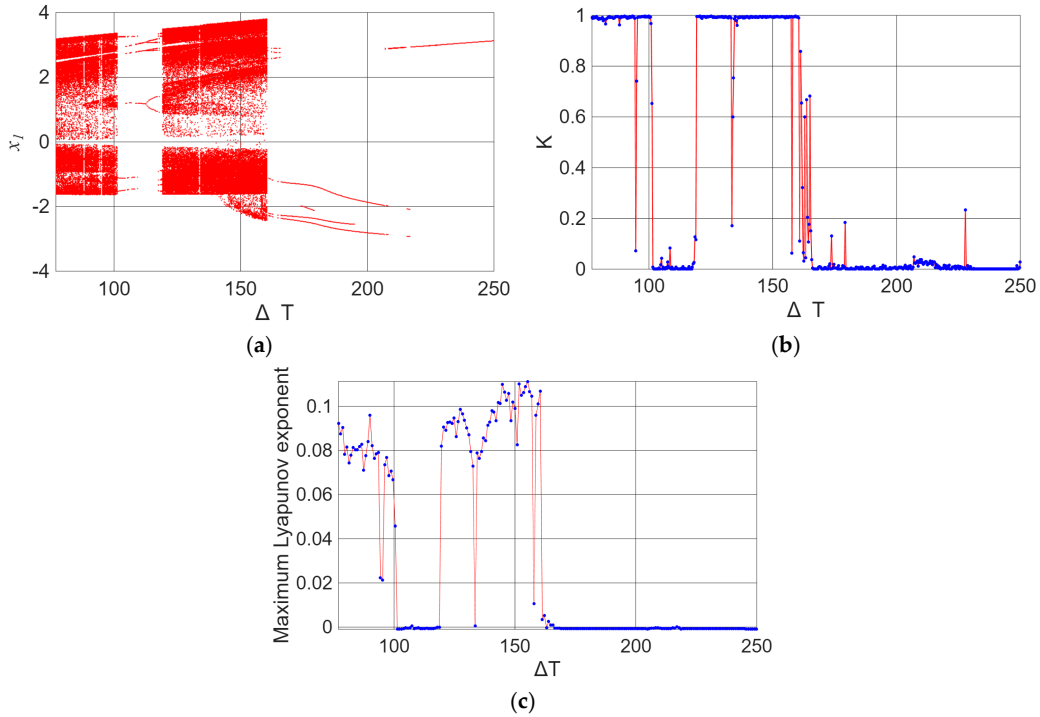

Figure 7. (**a**) Bifurcation Diagram for $\Delta T = [77 : 250]$. (**b**) 0–1 test for $\Delta T = [77 : 250]$. (**c**) Maximum Lyapunov exponent for $\Delta T = [77 : 250]$.

As shown in Figure 7, the tool temperature causes the behavior to alternate between chaotic (K close to 1, Figure 7a) and periodic (K close to 0, Figure 7a).

Figure 8 shows the time history, phase diagram, and Poincaré map for $\Delta T = 77$.

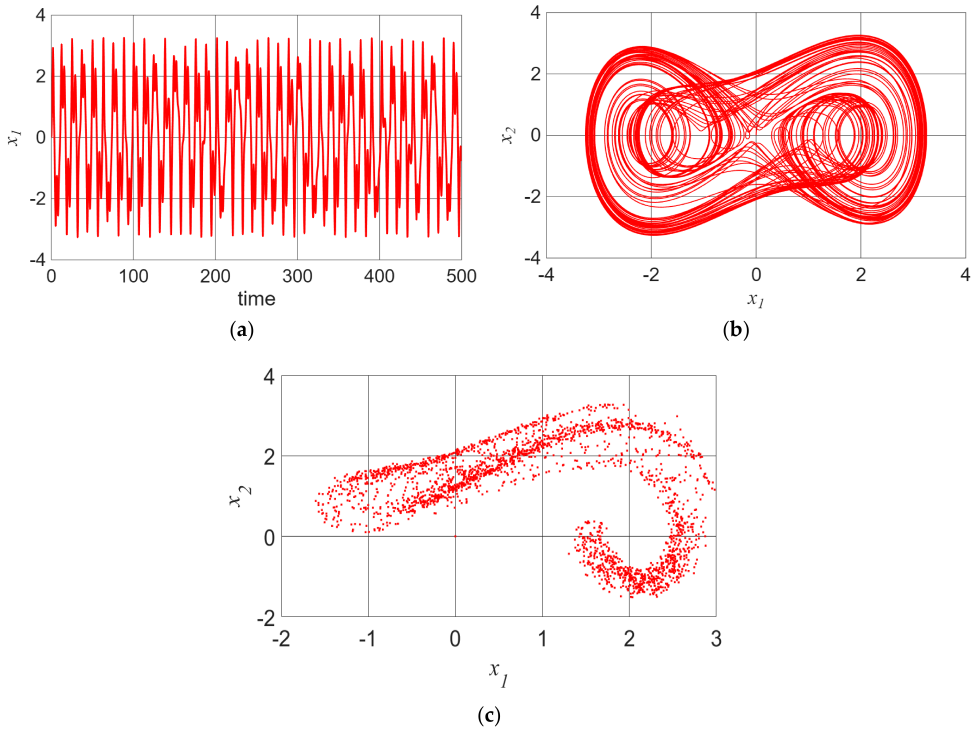

Figure 8. (**a**) Tool tip displacement (x_1) to $\Delta T = 77$. (**b**) Phase Diagram x_1 versus x_2 to $\Delta T = 77$. (**c**) Poincaré map for $\Delta T = 77$.

As observed for the ideal system, Figure 8 shows that at room temperature, the tool exhibits chaotic behavior during machining; however, as illustrated in Figure 7, the tool's behavior can alternate between periodic and chaotic states with temperature variations, provided the tool is made of a shape-memory alloy (SMA). If maintaining the temperature at a specific value is not feasible, the system can be managed through active or semi-active control.

Figure 9 shows the variations in the motor's angular displacement (x_3) and angular frequency (x_4), along with the corresponding phase diagram.

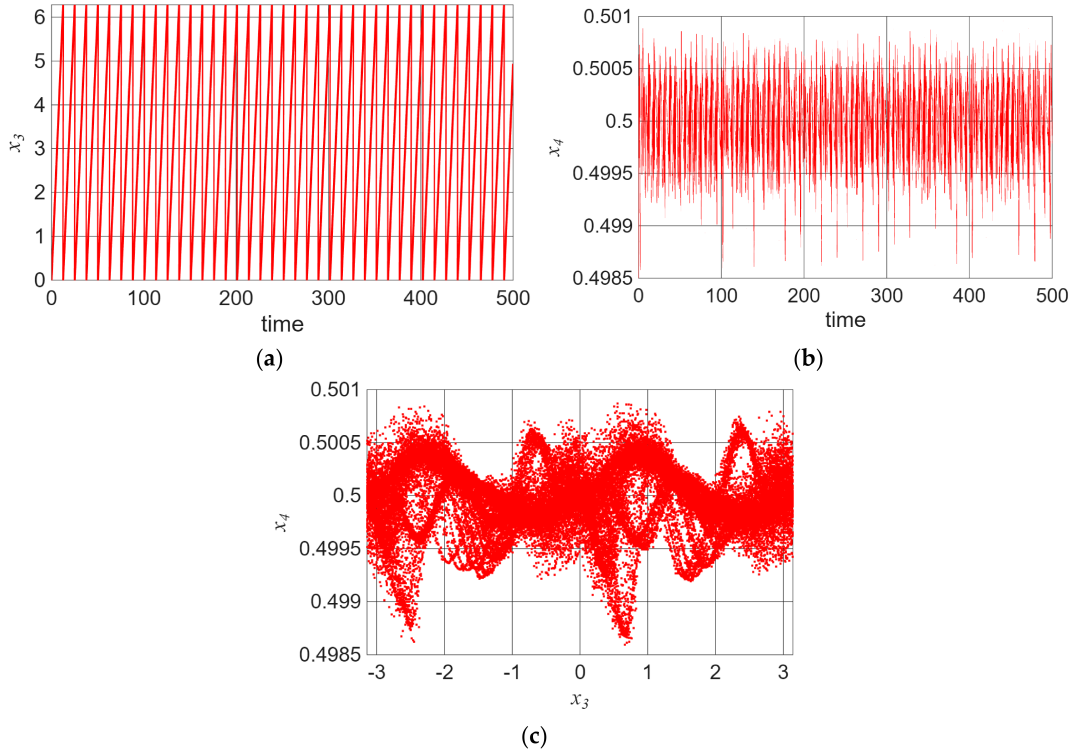

Figure 9. (**a**) Angular displacement x_3 to $\Delta T = 77$. (**b**) Angular frequency x_4 to $\Delta T = 77$. (**c**) Phase Diagram x_3 versus x_3 to $\Delta T = 77$.

As shown in Figure 9b, the motor's angular frequency x_4 is directly influenced by the tool's vibrations x_1, thereby reproducing the chaotic behavior shown in Figure 8a. This behavior is characteristic of non-ideal systems, in which a dynamic interaction occurs between the excitation source and the mechanical structure; the structure's oscillations influence the motor's dynamics and, consequently, its angular frequency.

Figure 10 illustrates the influence of the parameter β_2, which represents the electrical voltage applied to the motor's armature, on the motor's angular frequency x_4 and the beam's vibratory response x_1. This analysis enables evaluation of how variations in the supply voltage affect the system's dynamic behavior, accounting for the electromechanical coupling between the motor and the structure. Specifically, the aim is to identify how changes in β_2 affect the dynamics of the excitation source and, in turn, the amplitude and characteristics of the tool's vibrations.

As shown in Figure 10, the variable x_1, representing the tool's vibratory displacement, exhibits a jump in its dynamic response at $\beta_2 = 56.5$, when the motor angular frequency, x_4, reaches 0.282. This behavior indicates a significant change in the system's dynamics, suggesting a potential transition between oscillation regimes. This phenomenon may be linked to the nonlinear interaction between the excitation source and the mechanical structure, a characteristic feature of non-ideal electromechanical systems.

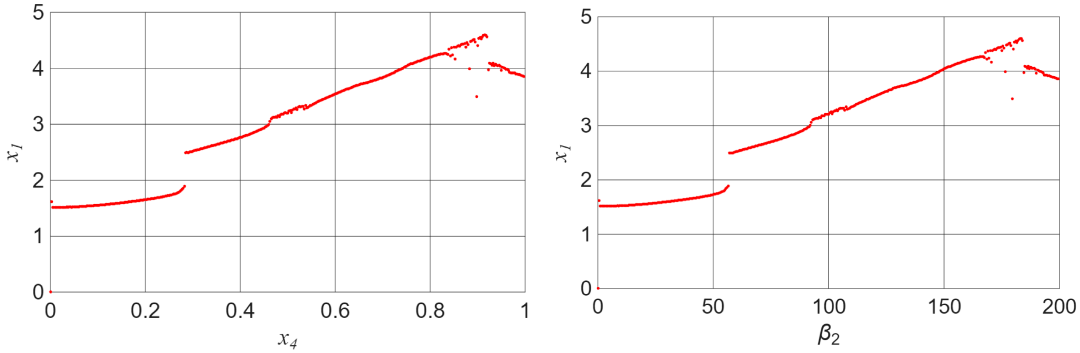

Figure 10. (**a**) Angular displacement x_3 to $\Delta T = 77$. (**b**) Angular frequency x_4 to $\Delta T = 77$.

Application of Time-Delayed Feedback Control

Considering the inclusion of a control signal U in the system (10), in the following form:

$$\begin{aligned}
\dot{x}_1 &= x_2 \\
\dot{x}_2 &= \frac{1}{1+\beta_1\delta_1 \sin(x_3)^2}\begin{pmatrix} -\alpha_1 x_2 - \alpha_2 x_1 - \alpha_3 {x_1}^3 - \alpha_4 {x_1}^5 \\ +\beta_2\delta_1 \sin(x_3) - \beta_3 x_4 \delta_1 \sin(x_3) + \delta_2 {x_4}^2 \cos(x_3) \end{pmatrix} + U \\
\dot{x}_3 &= x_4 \\
\dot{x}_4 &= \frac{1}{1+\beta_1\delta_1 \sin(x_3)^2}\begin{pmatrix} -\alpha_1 x_2 \beta_1 \sin(x_3) - \alpha_2 x_1 \beta_1 \sin(x_3) \\ -\alpha_3 {x_1}^3 \beta_1 \sin(x_3) - \alpha_4 {x_1}^5 \beta_1 \sin(x_3) + \\ \delta_2 {x_4}^2 \cos(x_3) \beta_1 \sin(x_3) + \beta_2 - \beta_3 x_4 \end{pmatrix}
\end{aligned} \tag{27}$$

Unlike the ideal system, where the excitation frequency is known, the non-ideal system requires estimating it. This paper considers the use of the FFT to determine the dominant excitation frequencies. In Figure 11, the FFT of the system (27) is shown.

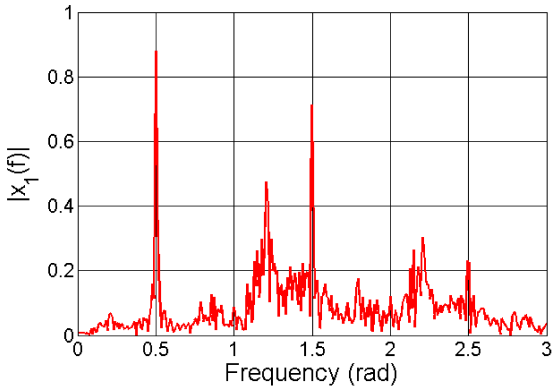

Figure 11. Fast Fourier Transform (FFT).

An analysis of the three main frequencies shown in Figure 11 reveals that the first is $\Omega = 0.5$ radians, associated with the motor's angular velocity. The second and third frequencies are $\Omega = 1.496$ rad and $\Omega = 1.208$ rad, respectively; both are associated with the cutting tool structure.

Considering the angular frequency $\Omega = 0.5$, we obtain the time delay $T = \frac{2\pi}{0.5} \approx 12.5664$.

In Figure 12, we can observe the bifurcation diagram for system (27) with control U, considering $T \approx 12.5664$ and variations in the control gain κ.

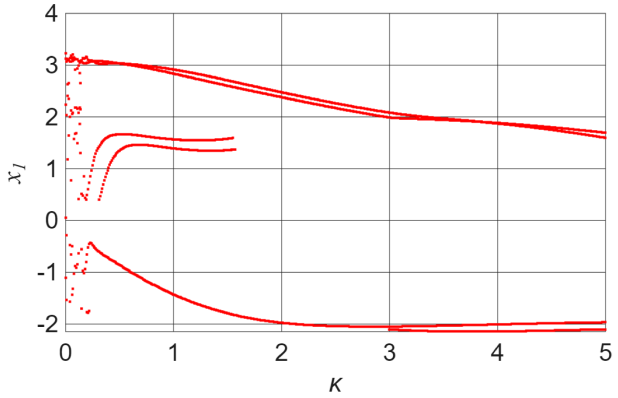

Figure 12. Bifurcation Diagram for $\kappa = [0 : 5]$.

We can observe in Figure 4 that the system with time-delay control for $T \approx 12.5664$ and $\kappa = 3.8$ shifts the system from chaotic behavior to periodic behavior. Substituting $T \approx 12.5664$ and $\kappa = 3.8$ into system (18), we obtain the control:

$$U = 3.8[x_2(\tau - 12.5664) - x_2(\tau)] \tag{28}$$

The time delay T is adjusted to $T = \frac{2\pi}{\Omega}$, where Ω represents one of the predominant excitation frequencies.

Figure 13 presents the time history and the control signal employed for the system (27), with control (28).

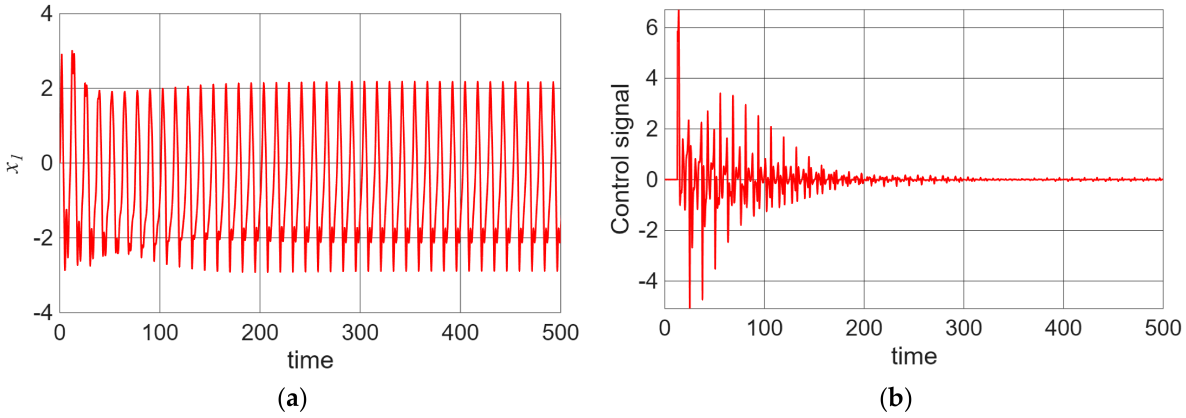

Figure 13. (**a**) Time history for non-ideal systems with control. (**b**) The control signal is applied in the control.

Figure 14 presents the time history and phase diagram for the system, both without and with control.

An analysis of the results presented in Figures 13 and 14 reveals that the proposed control scheme shifted the non-ideal system from chaotic to periodic behavior, mirroring the behavior observed in the ideal system. The control served to stabilize the system's dynamics on the periodic orbit. After approximately 300 time units, the control force approached zero, indicating that the periodic orbit was maintained without significant continuous intervention. Furthermore, as shown in Figure 14a, the control reduced the system's displacement amplitude by 22.19%.

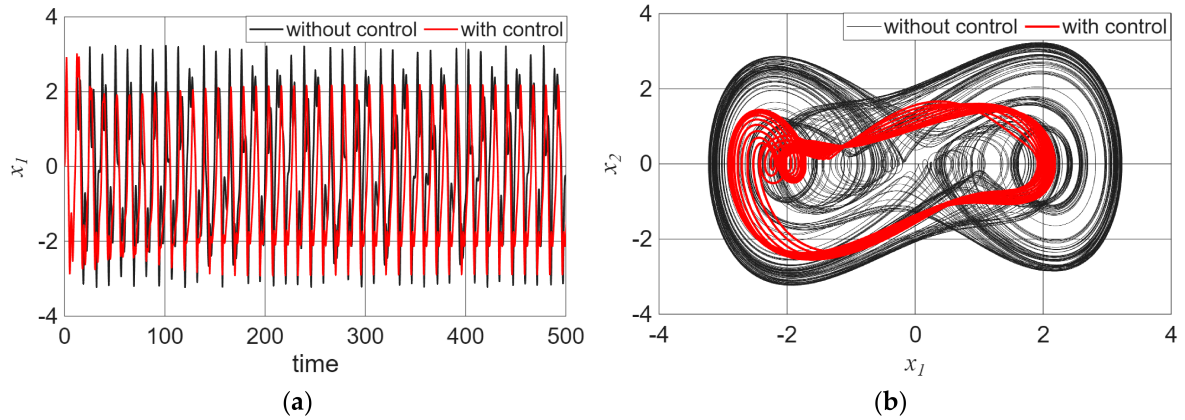

Figure 14. (**a**) Time histories for non-ideal systems, with and without control. (**b**) Phase Diagram x_1 versus x_2 for non-ideal systems without and with control.

3.3. Comparative Analysis of Ideal and Non-Ideal Systems

Figure 15 presents the time histories and phase diagrams for the ideal and non-ideal systems, both without control.

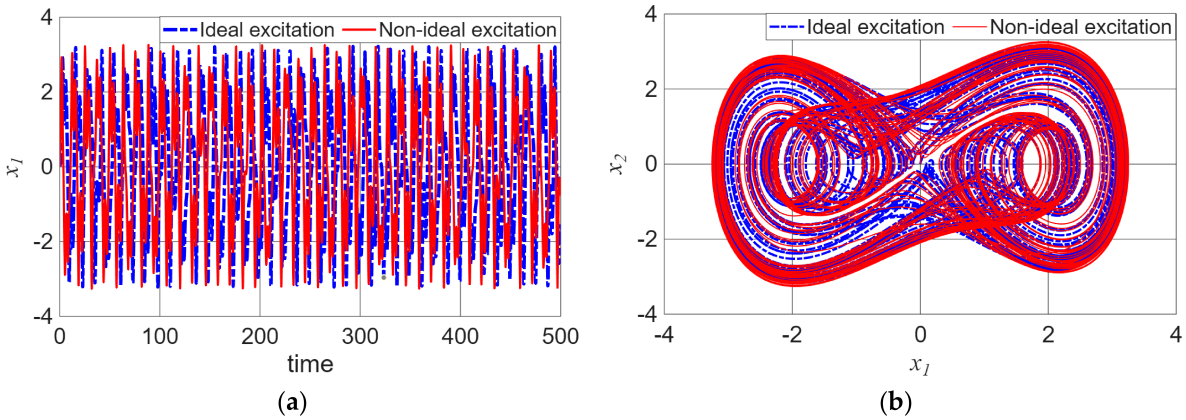

Figure 15. (**a**) Time history for ideal and non-ideal systems without control. (**b**) Phase Diagram x_1 versus x_2 for ideal and non-ideal systems without control.

As shown in Figure 15, the results indicate a small difference in the system's displacement amplitudes under ideal versus non-ideal excitation, with values of 6.43 and 6.51, respectively. However, despite the proximity of the maximum amplitudes, differences in frequency are observed, indicating that the nature of the excitation source influences the system's dynamic response.

Figure 16 presents the time history and signal of the control for the ideal and non-ideal system, both with control.

From the results in Figure 16, it can be observed that the controlled systems, when subjected to the same natural frequency, converge to similar dynamic behavior, even with different control gains. In both cases, the control drives the system toward one of its natural periodic orbits. In contrast, the control effort gradually decreases, tending toward zero as the system converges to that periodic orbit. These results indicate that the control acts primarily during the transition from the initial behavior to a natural periodic orbit of the system, without the need for sustained control once convergence is achieved.

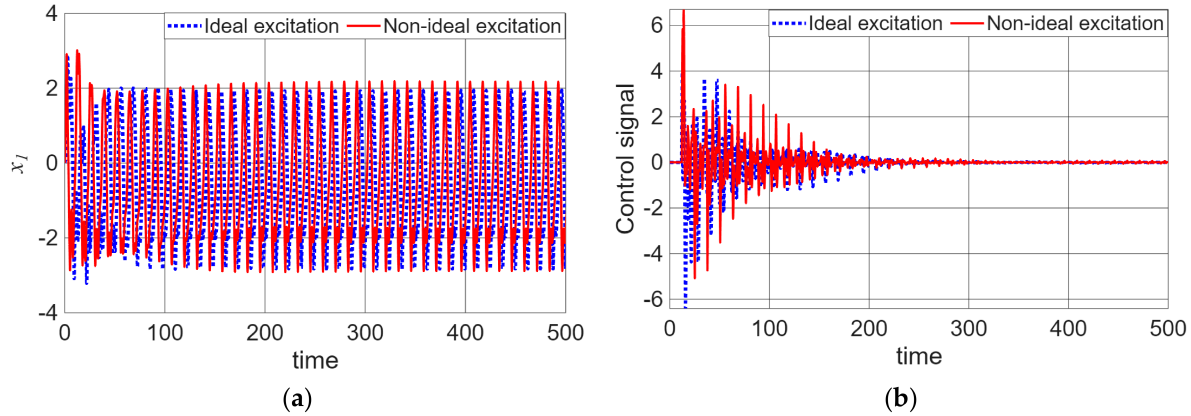

Figure 16. (**a**) Time history for non-ideal systems with control. (**b**) The control signal is applied to the control.

3.4. Sensitivity Analysis of Controllers to Variations in SMA Temperature

Figure 17 presents the bifurcation diagram and the 0–1 test for the ideal and non-ideal systems, both with control and temperature variations $\Delta T = [77 : 250]$.

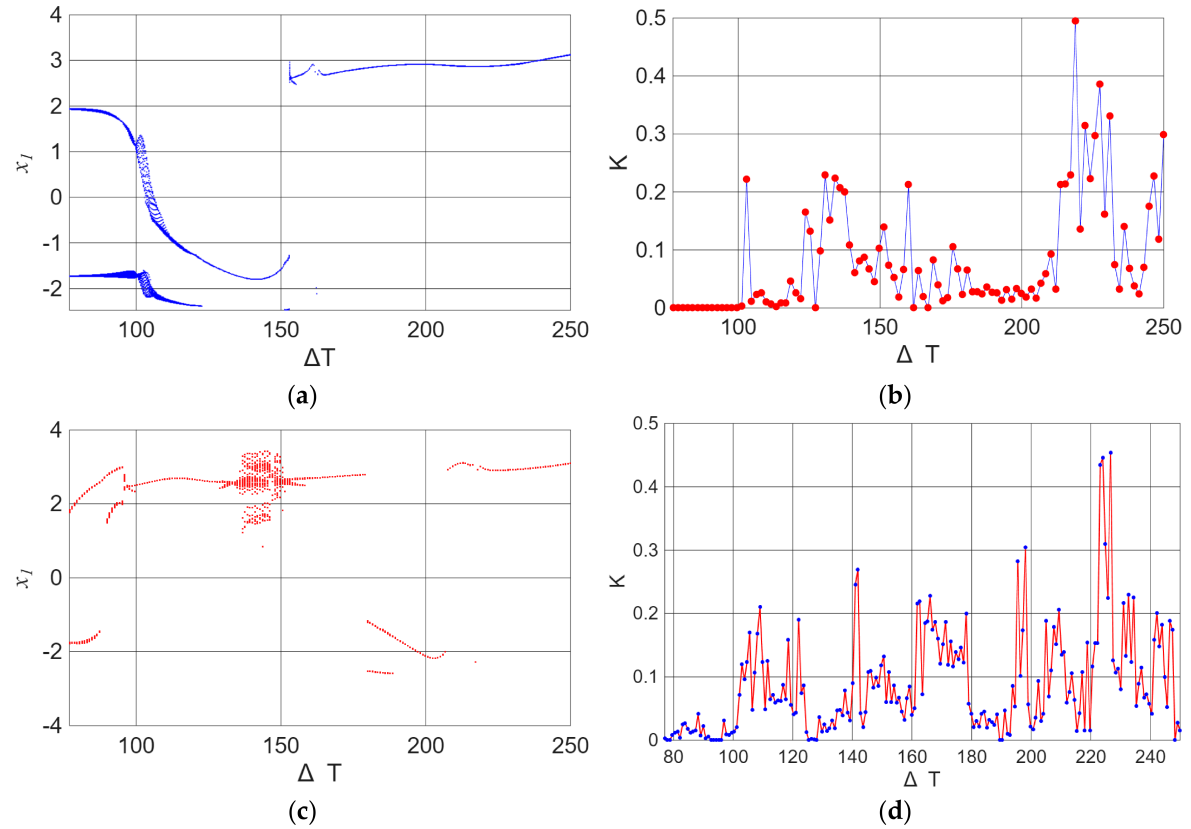

Figure 17. (**a**) Bifurcation Diagram for ideal excitation. (**b**) 0–1 test for ideal excitation. (**c**) Bifurcation Diagram for non-ideal excitation. (**d**) 0–1 test for non-ideal excitation.

Analyzing Figure 17b,c, it can be observed that all values of the parameter K remain below 0.5, indicating that the controlled system, considering $\Delta T = 77$, maintains periodic behavior across the analyzed temperature variations, without reverting to chaotic behavior. Furthermore, a comparative analysis of the bifurcation diagrams presented in Figure 17a,c reveals that the sensitivity of the control to temperature variations depends on the type of excitation considered. For ideal excitation, this sensitivity is most evident in

the range $100 < \Delta T < 110$, whereas for non-ideal excitation, it occurs predominantly in the range $135 < \Delta T < 155$. These results demonstrate that the nature of the excitation source influences the robustness of the control under temperature variations in the shape-memory alloy (SMA).

3.5. Sensitivity Analysis of Controllers to Variations in Delay Time (T)

Because the time delay in the control strategy is directly related to one of the system's excitation frequencies, selecting that frequency can significantly affect the controller's efficiency. Furthermore, time-delay values other than those determined by the relationship ($T = \frac{2\pi}{\Omega}$) may lead to less efficient control performance.

Thus, to evaluate the robustness and sensitivity of the control strategy to the choice of time delay, variations of ±20% around the nominal time-delay value will be considered. For each condition investigated, the time-domain displacement response x_1 and variations in the control signal U will be analyzed to assess both the efficiency of vibration attenuation and the influence of these variations on the control effort.

Figure 18 presents the time-domain responses of the displacement x_1 and the control signal U, considering ±20% variations in the time delay T relative to its nominal value. This analysis is conducted for the ideal system to investigate the sensitivity of the control strategy to variations in the time-delay parameter. The aim is to evaluate how these changes affect the efficiency of vibration attenuation, as well as the characteristics and intensity of the control signal required to maintain system performance.

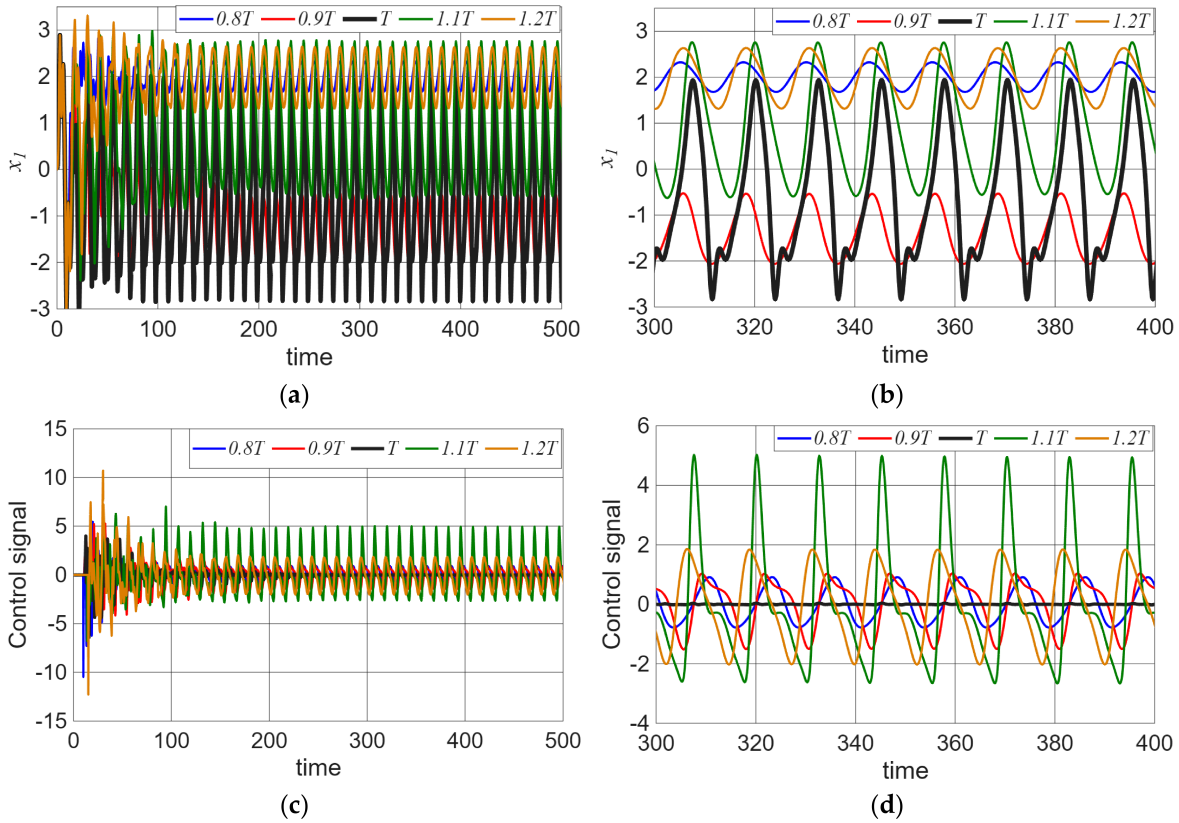

Figure 18. Ideal system. (**a**) Time history of x_1. (**b**) Time history of x_1, removing the transient from the system. (**c**) Variation in the control signal U. (**d**) Variation in the control signal U, removing the transient from the system.

Tables 1 and 2 present the minimum and maximum values, along with the corresponding ranges of variation, for the displacement x_1 and the control signal U, based on the results

shown in Figures 18b and 18d, respectively. These values quantify the influence of ±20% variations in the time delay T on the system's vibratory response and the magnitude of the control effort, thereby enabling an assessment of the sensitivity and robustness of the control strategy to changes in the time-delay parameter.

Table 1. Influence of the variation in the delay time (T) used in the control on the tool displacement (x_1).

Ideal System	$T = 10.0531$ −20%	$T = 11.3097$ −10%	$T = 12.5664$ 0%	$T = 13.8230$ −10%	$T = 15.0796$ −20%
min	1.6781	−2.0615	−2.8327	−0.6283	1.3118
max	2.3228	−0.5267	1.9447	2.7621	2.6347
Amplitude	0.6447	1.5349	4.7775	3.3904	1.3229

Table 2. Influence of the variation in the delay time (T) used in the control on the control signal (U).

Ideal System	$T = 10.0531$ −20%	$T = 11.3097$ −10%	$T = 12.5664$ 0%	$T = 13.8230$ −10%	$T = 15.0796$ −20%
min	−0.7823	−1.5163	−0.0222	−2.6637	−2.0258
max	0.9110	1.0393	0.0396	5.0179	1.8568
Amplitude	1.6934	2.5556	0.0618	7.6816	3.8825

Based on an analysis of the results presented in Figure 18 and Tables 1 and 2 for the ideal system, it is observed that, even with variations of ±20% in the nominal delay time T, the control strategies were able to suppress the system's chaotic behavior, maintaining its dynamic response within a periodic orbit. However, using delay values other than the nominal one leads to a significant increase in the amplitude of the control signal U, indicating that a greater control effort is required to keep the system in a periodic regime. Furthermore, a shift in the center of oscillation relative to the origin is observed, highlighting changes in the system's dynamic response. These results demonstrate that while the control strategy retains its ability to suppress chaotic behavior under the investigated variations, its performance is sensitive to the choice of delay time, particularly with respect to the required control effort and the position of the resulting periodic orbit.

As in the analysis of the ideal system, whose results are presented in Figure 18, Figure 19 shows the time responses of the displacement x_1 and the control signal U for the non-ideal system, considering ±20% variations in the delay time T relative to its nominal value. The objective is to investigate the influence of these variations on the control strategy's performance, evaluating its ability to suppress chaotic behavior arising from the coupling between the excitation source and the mechanical structure, as well as changes in the control effort required to maintain the system in a stable dynamic regime.

As in Tables 1 and 2 for the ideal system, Tables 3 and 4 present the minimum and maximum values, along with the corresponding oscillation amplitudes, for the displacement x_1 and the control signal U in the non-ideal system, based on the results shown in Figures 19b and 19d, respectively. These parameters quantify the effects of ±20% variations in the time delay T on the vibratory response and the control effort, allowing assessment of the control strategy's sensitivity to uncertainties in the time delay under non-ideal electromechanical coupling.

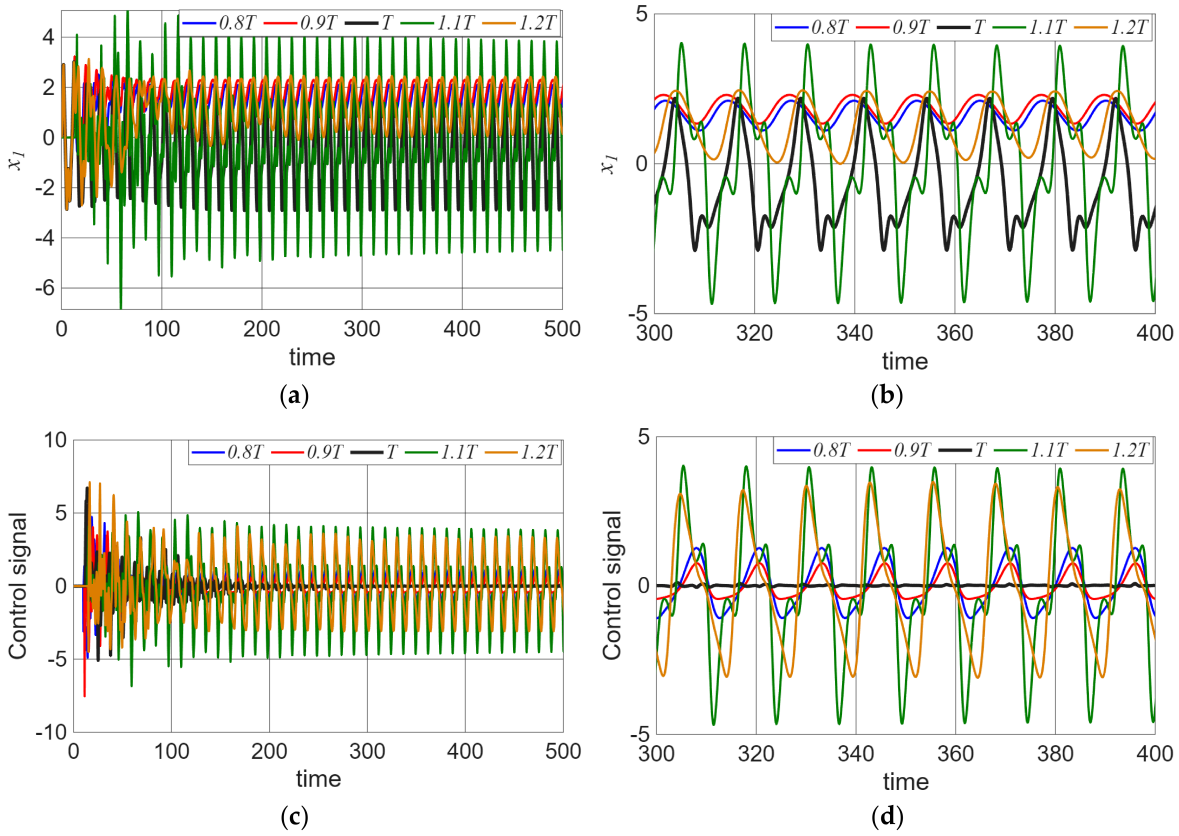

Figure 19. Non-ideal system. (**a**) Time history of x_1. (**b**) Time history of x_1, removing the transient from the system. (**c**) Variation in the control signal U. (**d**) Variation in the control signal U, removing the transient from the system.

Table 3. Influence of the variation in the delay time (T) used in the control on the tool displacement (x_1).

Non-Ideal System	$T = 10.0531$ −20%	$T = 11.3097$ −10%	$T = 12.5664$ 0%	$T = 13.8230$ −10%	$T = 15.0796$ −20%
min	1.1059	1.3388	−2.8937	−4.6795	−0.0045
max	2.1005	2.2949	2.1844	4.0280	2.4495
Amplitude	0.9946	0.9560	5.0780	8.7075	2.4540

Table 4. Influence of the variation in the delay time (T) used in the control on the control signal (U).

Non-Ideal System	$T = 10.0531$ −20%	$T = 11.3097$ −10%	$T = 12.5664$ 0%	$T = 13.8230$ −10%	$T = 15.0796$ −20%
min	−1.0927	−0.4520	−0.0620	−4.6795	−3.0951
max	2.1005	2.2949	2.1844	4.0280	2.4495
Amplitude	3.1932	2.7468	2.2464	8.7075	5.5446

Analysis of the results presented in Figure 19 and Tables 3 and 4 for the non-ideal system shows, much like the behavior identified in the ideal system, that the control strategies suppress chaotic behavior even in the presence of ±20% variations in the nominal time delay T, thereby maintaining the dynamic response within a periodic orbit. However, using time delays other than the nominal value significantly increases the amplitude of the control signal U, indicating that a greater control effort is required to maintain the system in a

periodic regime. Furthermore, a shift in the center of oscillation relative to the origin is observed, indicating changes in the dynamic equilibrium position of the controlled response. These results demonstrate that, while the control strategy retains its ability to suppress chaotic behavior in the non-ideal system under the conditions investigated, its performance is sensitive to variations in the time delay, particularly regarding the control effort required and the characteristics of the resulting periodic orbit.

4. Conclusions

This study investigated the nonlinear dynamics of a machining system incorporating a shape-memory alloy (SMA) in the tool structure, considering both ideal and non-ideal excitation sources. The results demonstrated that the system exhibits chaotic behavior at room temperature, while variations in the SMA temperature can induce transitions between periodic and chaotic regimes. These findings highlight the influence of temperature-dependent material properties and excitation characteristics on the dynamic response of the machining system.

Time-delayed control (TDC) successfully suppressed chaotic oscillations and stabilized the system on periodic orbits under both excitation conditions. Under ideal excitation, the control reduced the maximum displacement amplitude by 41.32%, and the control force tended toward zero after approximately 250 time units. Under non-ideal excitation, the maximum displacement amplitude decreased by 22.19%, and the control force approached zero after about 300 time units. These results indicate that the proposed strategy can stabilize periodic motion and requires negligible control effort once convergence is achieved.

Although the controlled systems exhibited similar displacement amplitudes, differences in oscillation frequencies revealed the influence of the excitation source on the system's dynamic response. Furthermore, a sensitivity analysis of temperature showed that the controller's robustness depends on both the excitation condition and the SMA's temperature range. Within the investigated ranges, the system maintained periodic behavior despite temperature variations, although distinct regions of higher sensitivity were identified for both ideal and non-ideal excitation scenarios.

Overall, the results demonstrate the potential of TDC for controlling chaotic vibrations in SMA-based machining systems under various excitation conditions. A systematic comparison between ideal and non-ideal excitations provides a deeper understanding of how the interaction between the source and the structure influences nonlinear dynamics and control performance.

Future research should investigate additional mathematical models that more accurately capture the thermomechanical behavior of shape memory alloys (SMAs), including the effects of loading history and phase transformations. Additionally, it is recommended to examine the influence of uncertainties in machining process parameters and the system's sensitivity to variations in operating conditions. Such investigations will enable a more comprehensive assessment of the proposed approach's applicability, robustness, and reliability under real-world machining conditions. Finally, it is suggested that other control strategies be explored to improve suppression of regenerative vibrations and enhance the system's dynamic stability across various operating conditions.

Author Contributions: Conceptualization, A.M.T. and J.M.B.; methodology, D.I., G.G.L. and V.H.J.; validation, D.I., G.G.L. and A.M.T.; formal analysis, V.H.J. and J.M.B.; investigation, A.M.T., D.I., J.M.B., V.H.J. and G.G.L.; writing—original draft preparation, A.M.T. and J.M.B.; writing—review and editing, D.I., V.H.J., G.G.L. and A.M.T.; visualization, D.I. and V.H.J.; supervision, A.M.T.; project administration, A.M.T. All authors have read and agreed to the published version of the manuscript.

Funding: The first author thanks CNPq for the financial support (Process: 305009/2026-5). The third author thanks CNPq for the financial support (Process: 309799/2021-0). The fifth author thanks CNPq for the financial support (Process: 303551/2026-7).

Institutional Review Board Statement: Not applicable.

Informed Consent Statement: Not applicable.

Data Availability Statement: The original contributions presented in this study are included in the paper. Further inquiries can be directed to the corresponding author.

Acknowledgments: The authors thank CAPES, Fundação Araucária, and CNPq. During the preparation of this manuscript, the authors used the software Grammarly for Windows, to correct and structure the text. The authors have reviewed and edited the output and take full responsibility for the content of this publication.

Conflicts of Interest: The authors declare no conflicts of interest.

References

1. Wang, A.; Zhou, B.; Jin, W. Dynamics of the regenerative turning chatter with little mass eccentricity. *Int. J. Non-Linear Mech.* **2024**, *166*, 104851. [CrossRef]
2. Kecik, K.; Rusinek, R.; Warminski, J. Modeling of high-speed milling process with frictional effect. *Proc. Inst. Mech. Eng.-Part K J. Multi-Body Dyn.* **2013**, *227*, 3–11. [CrossRef]
3. Molnár, T.G.; Insperger, T.; Stépán, G. State-dependent distributed-delay model of orthogonal cutting. *Non-Linear Dyn.* **2016**, *84*, 1147–1156. [CrossRef]
4. Hardt, M.; Jayaramaiah, D.; Bergs, T. On the Application of the Particle Swarm Optimization to the Inverse Determination of Material Model Parameters for Cutting Simulations. *Modelling* **2021**, *2*, 129–148. [CrossRef]
5. Rusinek, R.; Weremczuk, A.; Warmiński, J. Regenerative model of cutting process with non-linear duffing oscillator. *Mech. Mech. Eng.* **2011**, *15*, 131–145.
6. Yan, Y.; Xu, J.; Wiercigroch, M. Regenerative chatter in a plunge grinding process with workpiece imbalance. *Int. J. Adv. Manuf. Technol.* **2017**, *89*, 2845–2862. [CrossRef]
7. Lu, K.; Gu, F.; Longstaff, A.; Li, G. An investigation into tool dynamics adaptation for chatter stability enhancement in the turning of flexible workpieces. *Int. J. Adv. Des. Manuf. Technol.* **2020**, *111*, 3259–3271. [CrossRef]
8. Mohammadi, Y.; Ahmadi, K. Chatter in milling with robots with structural nonlinearity. *Mech. Syst. Signal Process.* **2022**, *167*, 108523. [CrossRef]
9. Wang, M.; Qin, P.; Zan, T.; Gao, X.S.; Han, B.S.; Zhang, Y.L. Improving optimal chatter control of slender cutting tool through more accurate tuned mass damper modeling. *J. Sound Vib.* **2021**, *513*, 116393. [CrossRef]
10. Hayati, S.; Shahrokhi, M.; Hedayati, A. Development of a frictionally damped boring bar for chatter suppression in boring process. *Int. J. Adv. Manuf. Technol.* **2021**, *113*, 2761–2778. [CrossRef]
11. Li, X.; Wan, S.; Yuan, J.; Yin, Y.; Hong, J. Active suppression of milling chatter with LMI-based robust controller and electromagnetic actuator. *J. Mater. Process. Technol.* **2021**, *297*, 117238. [CrossRef]
12. Saleh, M.K.A.; Ulasyar, A.; Lazoglu, I. Active damping of chatter in the boring process via variable gain sliding mode control of a magnetorheological damper. *CIRP Ann.* **2021**, *70*, 337–340. [CrossRef]
13. Muhammad, B.B.; Bashir, M.; Hamza, M.F.; Abdulhadi, M.; Shehu, M.A.; Debnath, S.K.; Bagchi, S. A feedback controller for milling chatter vibration control using a new response matrix. *J. Vib. Control* **2022**, *28*, 998–1010. [CrossRef]
14. Liu, S.; Xiao, J.; Tian, Y.; Ma, S.; Liu, H.; Huang, T. Chatter-free and high-quality end milling for thin-walled workpieces through a follow-up support technology. *J. Mater. Process. Technol.* **2023**, *312*, 117857. [CrossRef]
15. Navarro-Devia, J.H.; Chen, Y.; Dao, D.V.; Li, H. Chatter detection in milling processes—A review on signal processing and condition classification. *Int. J. Adv. Manuf. Technol.* **2023**, *125*, 3943–3980. [CrossRef]
16. Ding, B.; Kong, J.; Wang, W.; Wang, Z.; Xiao, J.; Zhang, Q. Investigation on a semi-active vibration attenuation device with follow-up support technology for mirror milling of thin-walled workpieces. *Mech. Syst. Signal Process.* **2025**, *224*, 112053. [CrossRef]
17. Li, Y.; Li, B.; Zhao, W.; Tian, W.; Liao, W. Design of an intelligent vibration damping fixture for robotic machining of thin-walled parts. *Mechatronics* **2025**, *109*, 103333, 2025. [CrossRef]
18. Mei, N.; Zhao, Z.; Lin, L.; Yu, Y.; Xu, J. Milling vibration suppression mechanism and stability analysis by introducing the spiral acoustic black hole as a vibration absorber in milling thin-walled parts. *Chin. J. Mech. Eng.* **2026**, 100379. [CrossRef]

19. Ozsoy, M.; Sims, N.D.; Ozturk, E. Actuator saturation during active vibration control of milling. *Mech. Syst. Signal Process.* **2025**, *224*, 111942. [CrossRef]
20. Singaravelu, C.; Varatharjan, P.; Ramu, G.; Alagappan, K. Investigation of damping characteristics on copper-based shape memory alloy frictional damper in boring process. *Arab. J. Sci. Eng.* **2021**, *46*, 11859–11870. [CrossRef]
21. Falk, F.; Konopka, P. Three-dimensional Landau theory describing the martensitic phase transformation of shape-memory alloys. *J. Phys. Condens. Matter* **1990**, *2*, 61–77. [CrossRef]
22. Piccirillo, V.; Balthazar, J.M.; Pontes, B.R., Jr.; Felix, J.L.P. Control of a Nonlinear Oscillator with Shape Memory Alloy Using an Optimal Linear Control: Part I: Ideal Energy Source. *Nonlinear Dyn.* **2009**, *55*, 139–149. [CrossRef]
23. Janzen, F.C. Positioning and Vibration Control of a Flexible Structure in Slewing Motion by Applying Shape Memory Alloys. Ph.D. Thesis, São Paulo State University (UNESP), Bauru, SP, Brazil, 2016.
24. Qu, R.; Li, S.; Bi, Q. Forced vibration of shape memory alloy spring oscillator and the mechanism of sliding bifurcation with dry friction. *Adv. Mech. Eng.* **2019**, *11*, 1–15. [CrossRef]
25. Balthazar, J.M.; Tusset, A.M.; Brasil, R.M.L.R.F.; Felix, J.L.P.; Rocha, R.T.; Janzen, F.C.; Nabarrete, A.; Oliveira, C. An Overview on the Appearance of the Sommerfeld Effect and Saturation Phenomenon in Non-Ideal Vibrating Systems (NIS) in Macro and MEMS Scales. *Nonlinear Dyn.* **2018**, *93*, 19–40. [CrossRef]
26. Pyragas, K. Continuous control of chaos by self-controlling feedback. *Phys. Lett. A* **1992**, *170*, 421–428. [CrossRef]
27. Tusset, A.M.; Ribeiro, M.A.; Lenz, W.B.; Rocha, R.T.; Balthazar, J.M. Time Delayed Feedback Control Applied in an Atomic Force Microscopy (AFM) Model in Fractional-Order. *J. Vib. Eng. Technol.* **2020**, *8*, 327–335. [CrossRef]
28. Gottwald, G.; Melbourne, I. A new test for chaos in deterministic systems. *Proc. R Soc. Lond. A* **2004**, *460*, 603–611. [CrossRef]
29. Gottwald, G.A.; Melbourne, I. The 0-1 Test for Chaos: A Review. In *Chaos Detection and Predictability*; Skokos, C., Gottwald, G., Laskar, J., Eds.; Lecture Notes in Physics; Springer: Berlin/Heidelberg, Germany, 2016; Volume 915. [CrossRef]

Disclaimer/Publisher's Note: The statements, opinions and data contained in all publications are solely those of the individual author(s) and contributor(s) and not of MDPI and/or the editor(s). MDPI and/or the editor(s) disclaim responsibility for any injury to people or property resulting from any ideas, methods, instructions or products referred to in the content.